

1 Impacts of Forest Fire Ash on Aquatic Mercury Cycling

2 Han-Han Li, Martin Tsz-Ki Tsui,* Peijia Ku, Huan Chen, Ziyu Yin, Randy A. Dahlgren, Sanjai J. Parikh,
3 Jianjun Wei, Tham C. Hoang, Alex T. Chow, Zhang Cheng* and Xue-Mei Zhu*



Cite This: <https://doi.org/10.1021/acs.est.2c01591>



Read Online

ACCESS |



Metrics & More



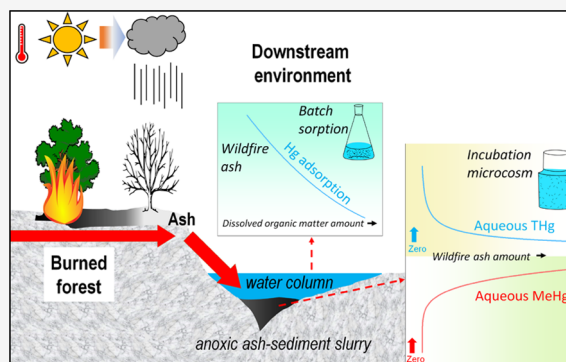
Article Recommendations



Supporting Information

4 **ABSTRACT:** Mercury (Hg) is a ubiquitous contaminant in the
5 environment and its methylated form, methylmercury (MeHg), poses a
6 worldwide health concern for humans and wildlife, primarily through fish
7 consumption. Global production of forest fire ash, derived from wildfires
8 and prescribed burns, is rapidly increasing due to a warming climate, but
9 their interactions with aqueous and sedimentary Hg are poorly
10 understood. Herein, we compared the differences of wildfire ash with
11 activated carbon and biochar on the sorption of aqueous inorganic Hg
12 and sedimentary Hg methylation. Sorption of aqueous inorganic Hg was
13 greatest for wildfire ash materials (up to 0.21 and 2.2 $\mu\text{g g}^{-1}$ C) among all
14 of the solid sorbents evaluated. A similar Hg adsorption mechanism for
15 activated carbon, biochar made of walnut, and wildfire ash was found that
16 involves the formation of complexes between Hg and oxygen-containing
17 functional groups, especially the $-\text{COO}$ group. Notably, increasing dissolved organic matter from 2.4 to 70 mg C L^{-1} remarkably
18 reduced Hg sorption (up to 40% reduction) and increased the time required to reach Hg–sorbent pseudo-equilibrium. Surprisingly,
19 biochar and wildfire ash, but not activated carbon, stimulated MeHg production during anoxic sediment incubation, possibly due to
20 the release of labile organic matter. Overall, our study indicates that while wildfire ash can sequester aqueous Hg, the leaching of its
21 labile organic matter may promote production of toxic MeHg in anoxic sediments, which has an important implication for potential
22 MeHg contamination in downstream aquatic ecosystems after wildfires.

23 **KEYWORDS:** wildfire ash, activated carbon, biochar, aqueous mercury sorption, mercury methylation



24 ■ INTRODUCTION

25 Forest fires, including both wildfire and prescribed fires, are
26 important drivers of biogeochemical alterations to forest
27 ecosystems.¹ The frequency and intensity of wildfires are
28 rapidly increasing, partly attributable to global climate change,²
29 while prescribed fire is also becoming more prevalent as a
30 forest management tool.³ Further, these fires of various
31 intensities and durations have produced various effects on
32 the biogeochemical cycles of downstream aquatic systems,
33 such as carbon and nitrogen cycling.⁴

34 Mercury (Hg) is a pollutant of global concern as it
35 contaminates all geographical areas owing to its widespread
36 emissions (e.g., both natural and anthropogenic), long-range
37 atmospheric transport, and dry/wet deposition.⁵ Forest
38 ecosystems are an important sink of Hg due to enhanced
39 sequestration via foliar uptake⁶ and can also become a source
40 of Hg during/after forest fires via volatilization (for
41 atmospheric transport) and runoff/erosion (to aquatic
42 ecosystems).⁷ While much of the Hg in biomass has been
43 shown to be volatilized during forest fires,⁸ the remaining ash
44 may still contain significant amounts of Hg derived from the
45 burned vegetation.⁹ For example, total Hg concentrations up
46 to 125 ng g^{-1} dry wt were measured in ash after a northern
47 California wildfire, which would be even higher than litter (up

to 40 ng g^{-1}) and dead woody materials collected in a nearby 48
site (up to 57 ng g^{-1}).⁹ 49

In aquatic sediments, the methylation of inorganic Hg 50
[Hg(II)] by anaerobic bacteria produces highly toxic 51
methylmercury [MeHg].¹⁰ Mercury methylation is a key step 52
for Hg to enter the base of aquatic food webs, and 53
subsequently MeHg biomagnifies along the food chain, leading 54
to unsafe levels for the top aquatic predators.¹¹ Recently, Ku et 55
al.⁹ demonstrated that wildfire ash materials are capable of 56
effectively sequestering Hg(II) from natural waters and 57
evaluated the interactive behavior of ash and Hg with respect 58
to a few ash properties [e.g., percent loss-on-ignition (LOI) 59
and aromatic hydrocarbon (ArH) fraction], raising an 60
important but largely unanswered question: How might forest 61
fire ash interact with aqueous Hg(II) and mediate sedimentary 62
Hg methylation after fire events? 63

Interactions of Hg with wildfire ash provide an interesting 64
comparison to the numerous studies in the last few decades 65
examining the effectiveness of activated carbon and biochars 66

Received: March 5, 2022

Revised: June 21, 2022

Accepted: July 20, 2022

67 on the removal of aqueous Hg(II) and inhibition of Hg
68 methylation in sediments. For example, an early study
69 demonstrated the efficient removal of Hg(II) by activated
70 carbon.¹² Recently, Gilmour et al.¹³ showed the effectiveness
71 of activated carbon in mitigating MeHg formation in Hg-
72 contaminated sediments, while Gilmour et al.¹⁴ successfully
73 applied activated carbon in remediation of a Hg-contaminated
74 saltmarsh. Similarly, the use of biochar has been widely
75 evaluated, mostly in the laboratory, for removing aqueous
76 Hg^{15–19} and reducing Hg methylation in sediment/soil and
77 subsequent MeHg bioaccumulation.^{20,21}

78 While the precise mechanism of Hg(II) sorption by wildfire
79 ash is currently unknown,⁹ previous studies have posited a
80 similar mechanism for Hg sorption for both activated carbon
81 and biochar, specifically the formation of (COO)₂Hg and
82 (O)₂Hg complexes.¹⁹ However, a myriad of environmental
83 factors may compromise the effectiveness of these sorbents for
84 Hg removal, such as dissolved organic matter (DOM). DOM
85 has been recently shown to reduce the effectiveness of
86 activated carbon and biochar in sequestering aqueous Hg(II),
87 presumably through formation of aqueous Hg-DOM com-
88 plexes via the thiol group.^{22,23} It may be worth noting that no
89 study of Hg sequestration by wildfire ash has evaluated the
90 impact of different DOM concentrations and that DOM has
91 consistently been documented to increase in aquatic systems
92 post-wildfire.²⁴ Thus, complex biogeochemical interactions
93 must be considered when evaluating how solid-phase sorbents
94 (e.g., wildfire ash) interact with Hg in natural aquatic
95 environments (e.g., different DOM levels).

96 Due to the increasing extent of global wildfires^{2,25} and the
97 use of prescribed burning for forest management,³ there is an
98 urgent need to better understand how these solid-phase
99 sorbents mediate Hg cycling in downstream aquatic environ-
100 ments, especially in a range of DOM levels. In this work, we
101 compared the effectiveness of two wildfire ash, four laboratory-
102 controlled burn ash, one commercial activated carbon, and two
103 biochar samples for aqueous Hg removal and sedimentary Hg
104 methylation. Our findings demonstrated strong sequestration
105 of aqueous Hg(II) by all solid sorbents, but there is potential
106 for the forest fire ash materials to stimulate microbial Hg(II)
107 methylation when incubated in anoxic sediments.

108 ■ MATERIALS AND METHODS

109 **Solid Sorbent Materials.** In this study, we used two
110 wildfire ash samples (sieved < 2 mm) produced by low-severity
111 wildfires, i.e., wildfire ash 1 (Wragg Fire, July 22–August 5,
112 2015, no rainfall prior to sampling) and wildfire ash 2 (Rocky
113 Fire, July 29–August 14, 2015, no rainfall prior to sampling),
114 in northern California, more details of wildfire site character-
115 istics and sampling information can be found in Table S1 and
116 Text S1. In a subset of experiments, we used ash samples
117 generated by laboratory-controlled burning (i.e., 250ox, 250py,
118 550ox, 550py) in a laboratory under different temperatures
119 (i.e., 250 and 550 °C) and the presence/absence of oxygen
120 [i.e., pyrolysis (py) vs thermal oxidation (ox)] from white fir
121 (*Abies concolor*) litter.²⁶ For comparison, we included a
122 commercially available activated carbon (−20 + 40 mesh, CAS
123 7440-44-0, Alfa Aesar, Lancashire, UK) that was also used in
124 our previous study.⁹ The size of activated carbon particles
125 ranged from 0.8 to 2.4 mm, which would be comparable to the
126 size of our sieved ash samples. Further, we assessed two
127 biochar samples (biochar_{walnut}—walnut shell/gasification and
128 biochar_{sawdust}—sawdust/hydropyrolysis)²⁷ with similar carbon

content (i.e., ~63% C), but very different Hg sorption
capacities based on our preliminary tests. All solid sorbents
were stored dry in the laboratory prior to use and analyzed for
total Hg [THg] to assess their native Hg content (see
Analytical Measurements section).

Aqueous Sorption. We evaluated the capability of the
solid sorbents to remove aqueous Hg(II) in which we
performed three experiments to examine the equilibrium
adsorption: the effects of initial Hg(II) levels (0.5–10 μg L^{−1}),
contact time (0.5–48 h), and different dissolved organic
carbon (DOC) sources/levels (low-, mid-, and high-DOC at
2.4, 33.4, and 69.5 mg C L^{−1}, respectively) on aqueous Hg(II)
sorption. Stock solutions with different DOC levels (i.e., “low-
DOC”, “mid-DOC”, and “high-DOC”) were generated in the
laboratory and/or collected from the field. Briefly, low-DOC
water was prepared as a synthetic freshwater in the laboratory
(i.e., moderately hard water).²⁸ Mid-DOC water was collected
from a freshwater wetland located in eastern North Carolina.
High-DOC water was produced by incubating natural leaf litter
of mixed deciduous species in the laboratory with low-DOC
water for 2 days. We filtered all three water types through a 0.7
μm filter (Whatman GF/F) prior to use. For all sorption
experiments, we prepared a stock solution of Hg(II) at 1 μg
mL^{−1} from reagent-grade HgCl₂ powder (Alfa Aesar) in
laboratory-purified water (Barnstead Nanopure; 18.2 MΩ·
cm^{−1}) and stored at 4 °C in the dark until use. Working
solutions with different Hg(II) concentrations were prepared
by diluting the stock solution with low-DOC, mid-DOC, and
high-DOC waters.

Prior to sorption tests, we assessed the interactions of Hg
and DOC between the solid sorbents and three DOC water
types. Specifically, 0.50 ± 0.05 g of each solid sorbent (note:
laboratory-controlled burn ash was not used in all tests due to
limited availability) was added to 100 mL of each DOC water
type in a 500 mL Erlenmeyer glass flask (performed in
triplicate) in which the ratio of sorbent mass to water volume
(i.e., 0.5%) would be comparable to another recent Hg
sorption study (e.g., 0.3).²² The initial pH of the test solution
was adjusted to 7.80 ± 0.10 with a benchtop pH meter
(Mettler Toledo), which would be similar to streamwater in
burned sites in northern California²⁴ and this pH value would
be similar to another Hg sorption study.²² All flasks were
continuously agitated on an orbital shaker at a rate of 200 rpm
at room temperature in the dark. After 48 h, the supernatant
was filtered through a 1.0 μm filter (Whatman GF/B), and the
filtrate was quantified for THg and DOC (see below).

First, we examined Hg(II) sorption to all solid sorbents with
an initial Hg(II) concentration of 1 μg L^{−1}, which would be
comparable to other aqueous Hg sorption studies (e.g., 2 μg
L^{−1})²² but much lower than earlier Hg sorption studies (e.g.,
2–20 mg L^{−1}).¹² Similar to the above conditions, we added
0.50 ± 0.05 g of each solid sorbent into 100 mL of different
DOC water types. The sorption test lasted for 48 h with
continuous agitation in the dark at room temperature, while
the initial pH was adjusted to 7.80 ± 0.10. Control
experiments without sorbents were included to account for
the error generated by the Hg(II) adsorption on the inner
surface of flasks. Equilibrium adsorption (q_e) of Hg was
calculated as

$$q_e = [(C_0 - C_e) \times V] / (m) \quad (1)$$

where q_e (μg g^{−1}) is the quantity of adsorbed Hg per unit mass
of sorbent, C_0 and C_e (μg L^{−1}) are the initial and equilibrium

191 Hg concentrations, respectively; V (L) is the solution volume;
192 and m is the dry mass of the solid sorbent in grams.

193 Since the carbon/organic carbon of the solid sorbent plays
194 an important role in Hg(II) adsorption process,¹⁹ thus, the
195 equilibrium quantity (q_{ec}) of adsorbed Hg per unit mass of C
196 for each sorbent was also calculated as

$$197 \quad q_e = [(C_0 - C_e) \times V] / (m \times C) \quad (2)$$

198 where q_{ec} ($\mu\text{g g}^{-1}$ C) is the quantity of adsorbed Hg per unit
199 mass of C; C_0 and C_e ($\mu\text{g L}^{-1}$) are the initial and equilibrium
200 Hg concentrations, respectively; V (L) is the solution volume;
201 m is the dry mass of the solid sorbent in grams; and C is the
202 fraction of carbon of each solid sorbent.

203 Second, we evaluated the effect of initial Hg(II) concen-
204 tration (C_0) using an adsorption isotherm approach with a
205 range of C_0 ($0.5\text{--}10 \mu\text{g L}^{-1}$) for each solid sorbent (except
206 laboratory-controlled burn ash), with the conditions as
207 described above. The adsorption capacity and equilibrium
208 constant were assessed by the Langmuir isotherm adsorption
209 model as

$$210 \quad q_e = (q_m \times K_L \times C_e) / (1 + K_L \times C_e) \quad (3)$$

211 where q_m ($\mu\text{g g}^{-1}$) is the maximum amount of adsorbed Hg per
212 unit mass of sorbent and k_L ($\text{L } \mu\text{g}^{-1}$) is the constant for the
213 Langmuir isotherm adsorption model.

214 Third, we investigated the effect of contact time on the
215 sorption of Hg(II) by the solid sorbents in the three DOC
216 water types (except laboratory-controlled burn ash). All
217 conditions were the same as above except that a 10 mL
218 aliquot was taken from the supernatant at selected time
219 intervals (0.5, 1, 4, 8, 12, 24, 48 h) to determine the remaining
220 aqueous Hg(II) concentrations.²⁹ Kinetic data were evaluated
221 using pseudo-first-order (eq 3) and pseudo-second-order (eq
222 4) formulations

$$223 \quad q_t = q_e (1 - e^{-k_1 t}) \quad (4)$$

$$224 \quad q_t = (k_2 \times q_e^2 \times t) / (1 + k_2 \times q_e \times t) \quad (5)$$

225 where q_t ($\mu\text{g g}^{-1}$) is the amount of adsorbed Hg(II) per unit
226 mass of sorbent at time t , and k_1 (h^{-1}) and k_2 ($\text{g } \mu\text{g}^{-1} \text{h}^{-1}$) are
227 the rate constants of the pseudo-first-order and pseudo-
228 second-order models, respectively.

229 **Sediment Incubation.** Sediment incubation experiments
230 were used to assess how the solid-phase sorbents affected both
231 aqueous and sedimentary Hg(II) concentrations and mediated
232 production of MeHg during anoxic incubation over 2 weeks.
233 The experimental design was similar to our previous studies
234 incubating litter only^{30,31} and wildfire ash only.⁹ However, we
235 included a Hg-contaminated sediment (THg: $13.4 \pm 0.8 \mu\text{g}$
236 g^{-1} dry wt.; MeHg: $3.5 \pm 0.3 \text{ ng g}^{-1}$ dry wt.) collected from
237 the historically contaminated South River (Virginia)³² in our
238 incubation experiment to demonstrate whether wildfire ash
239 would reduce sedimentary Hg(II) methylation effectively as
240 demonstrated for activated carbon in other studies.¹³

241 We conducted the incubation experiments using South River
242 water with each solid sorbent at concentrations of 1, 5, and
243 10% as dry mass of the sediment, but we only included the 5%
244 treatment for the laboratory-controlled burn ash due to limited
245 availability. Briefly, we placed both river water and sediment
246 (control without solid sorbent or mixed with different solid-
247 phase sorbent concentrations) (at a ratio of 10:1 v/w) into a
248 250 mL air-tight, sterile, Hg-free Nalgene poly(ethylene

terephthalate) glycol (PETG) bottle (similar to our previous 249
incubation experiments).^{9,30,31} Triplicate bottles were included 250
for all treatments. Bottles were tightly capped and placed in the 251
dark at room temperature ($\sim 22^\circ\text{C}$) for 2 weeks. The bottles 252
were thoroughly shaken every day to mix the slurry. Aqueous 253
samples were collected and passed through $1.0 \mu\text{m}$ Whatman 254
GF/B filter at the end of the 2-week incubation to measure 255
filtered THg, filtered MeHg, and DOC. To understand 256
inorganic Hg and MeHg partitioning between solid and 257
aqueous phases, post-incubation sediment samples from 5% 258
sorbent addition treatments were collected and freeze-dried for 259
subsequent THg and MeHg determination. 260

Spectroscopic Characterization. To gain further insight 261
into Hg sorption mechanisms, the morphology and micro- 262
structure of three solid sorbents, namely, activated carbon, 263
biochar_{walnut} and wildfire ash 1, were examined using a field- 264
emission scanning electron microscope (SEM, ZEISS Sigma). 265
Samples were prepared by mounting biosorbent materials onto 266
a conductive carbon tape and gently depositing nonadhesive 267
silver powder via a N_2 flow. Samples were imaged at an 268
accelerating voltage of 5 eV. X-ray photoelectron spectroscopy 269
(XPS) was conducted to determine the surface chemical 270
composition of activated carbon, biochar_{walnut} and wildfire ash 271
1 before and after sorption of aqueous Hg(II) at $1 \mu\text{g L}^{-1}$ in 272
the presence of DOM (with mid-DOC water) using an XPS- 273
ESCALAB Xi+ Thermo Scientific instrument with an Al $K\alpha$ 274
radiation source. The binding energies of spectra were 275
calibrated to a C 1s peak at 284.8 eV. 276

Analytical Measurements. Filtered aqueous samples were 277
analyzed for THg by transferring the water samples into an 278
acid-cleaned, 40 mL glass vial (Thermo Scientific), and the 279
samples were digested overnight with an acidic mixture of 280
potassium permanganate and potassium persulfate at 80°C .³³ 281
Filtered aqueous samples were analyzed for MeHg by 282
preserving the samples with 0.4% trace-metal-grade hydro- 283
chloric acid (Fisher Scientific)³⁴ and kept in the dark at 4°C 284
before distillation. We also measured the solution pH at the 285
end of the sorption and incubation trials using a daily- 286
calibrated pH meter (Mettler Toledo) and DOC with a total 287
organic carbon analyzer (Shimadzu). 288

All sediment samples were immediately frozen at -20°C 289
and subsequently lyophilized with a benchtop freezer dryer 290
(SP Scientific). The dry sediments were sieved through an 291
acid-cleaned 1 mm polypropylene mesh to remove larger 292
particles and measured THg and MeHg. Concentrations of 293
Hg(II) in the sediments were calculated by subtracting 294
measured MeHg from THg. To understand the effect of the 295
sorbents on inorganic Hg and MeHg partitioning, sediment- 296
water partition coefficients for both Hg(II) and MeHg 297
($\log K_{d,\text{Hg(II)}}$) were calculated as the sedimentary concentration 298
in ng kg^{-1} divided by the aqueous concentration in ng L^{-1} .¹³ 299
Total amount of THg and MeHg as well as alteration of 300
percentage of THg as MeHg (% MeHg) in each incubation 301
microcosm were calculated to assess the Hg methylation 302
potential of the sediment incubation experiment impacted by 303
sorbent addition.^{30,35} Detailed analytical procedures for THg 304
and MeHg both water and sediment and quality assurance data 305
can be found in Text S2. 306

Statistical Analyses. Nonlinear regression analysis was 307
performed using OriginPro 2021 (OriginLab Corporation, 308
Northampton, MA) since the linearization might result in an 309
inherent bias, diverse estimation errors, and fit distortions. 310
Hence, nonlinear modeling is considered a more robust 311

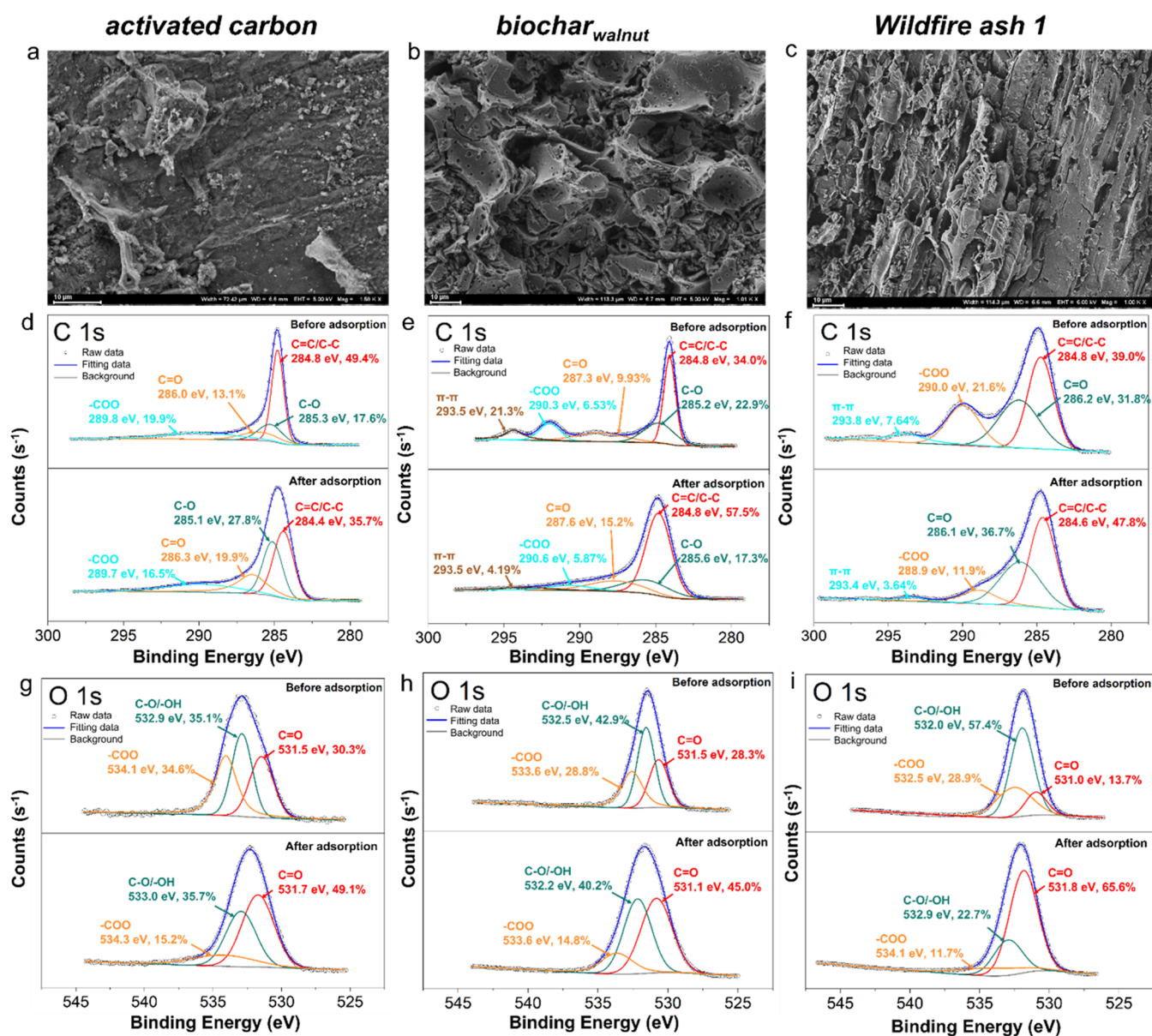


Figure 1. (a–c) SEM images of activated carbon, biochar_{walnut} and wildfire ash 1. (d–f) High-resolution XPS spectra of C 1s for activated carbon, biochar_{walnut} and wildfire ash 1 before and after reacting with Hg(II). (g–i) High-resolution XPS spectra of O 1s for activated carbon, biochar_{walnut} and wildfire ash 1 before and after Hg reactions.

312 approach for estimating kinetic and isotherm parameters.³⁶ All
 313 linear regression analyses were performed using OriginPro
 314 2021. One-way analysis of variance (ANOVA) with Student–
 315 Newman–Keuls multiple comparison tests was performed
 316 using SigmaPlot 12.5 (Systat Software, Palo Alto, CA). The
 317 significance level for all statistical analyses was set at $p = 0.05$.

318 ■ RESULTS AND DISCUSSION

319 **Basic Sorbent Characteristics and Hg–Sorbent**
 320 **Interactions.** There was a large range of C contents (10–
 321 71%) among the tested solid sorbents. Both activated carbon
 322 and biochars had >50% C contents, whereas laboratory-
 323 controlled burn ash had intermediate (13–43%) and wildfire
 324 ash the lowest (10–17%) C contents (Table S1). Notably,
 325 there was a large range of residual Hg contents (0.4–59.0 ng
 326 g⁻¹) in the solid sorbents, being much higher in both low-
 327 temperature laboratory-controlled burn and wildfire ashes than

those of activated carbon and biochars (2.6–10.6 ng g⁻¹).
 However, the laboratory-controlled burn ash generated at a
 high temperature (550ox and 550py) had negligible residual
 Hg (<1 ng g⁻¹) (Table S1).

SEM micrographs of the three representative sorbents
 (activated carbon, biochar_{walnut} and wildfire ash 1) indicated
 the prevalence of square morphologies and micropores with
 rough surfaces on activated carbon (Figure 1a). The
 biochar_{walnut} micrograph showed the presence of many large
 pores and different morphologic irregularities on the surface
 (Figure 1b). The SEM micrograph of the wildfire ash 1
 displayed a porous-folded structure (Figure 1c); such features
 can contribute to increased surface area and an elevated
 reactivity in interfacial reactions of the ash samples,³⁷
 potentially enhancing the aqueous sorption capability of
 Hg(II) by wildfire ash 1 (see results below).

344 XPS characterization of sorbent materials before and after
 345 reaction with aqueous Hg(II) displayed a clear Hg 4f peak for
 346 wildfire ash 1. In contrast, the Hg 4f peak for activated carbon
 347 and biochar_{walnut} was not clear, possibly owing to the low
 348 Hg(II) level ($1 \mu\text{g L}^{-1}$) used in this evaluation (Figure S1).
 349 The high-resolution Hg 4f spectra for activated carbon,
 350 biochar_{walnut} and wildfire ash 1 after Hg adsorption were
 351 fitted with a single Hg 4f spin-orbit split doublet (the Hg 4f_{5/2}
 352 and Hg 4f_{7/2} peaks).^{19,38} The reasons for the absence of a
 353 spin-orbit for Hg 4f are unknown, but doublet peaks appeared
 354 at 101.6 and 102.6 eV for activated carbon, 101.6 and 102.1 eV
 355 for biochar_{walnut}, and 100.7 and 101.6 eV for wildfire ash 1
 356 (Figure S1). The same peak at 101.6 eV revealed that Hg was
 357 adsorbed in a similar Hg form ($(-\text{COO})_2\text{Hg}$) by activated
 358 carbon, biochar_{walnut} and wildfire ash 1.

359 A shift of the binding energy for C 1s and O 1s was observed
 360 for activated carbon, biochar_{walnut} and wildfire ash 1 before and
 361 after Hg adsorption (Figure 1d–i and Table S2), implying the
 362 involvement of C- and/or O-containing functional groups in
 363 Hg adsorption.^{19,39} Strikingly, after Hg adsorption by activated
 364 carbon, biochar_{walnut} and wildfire ash 1, the carboxylic
 365 ($-\text{COO}$) group in O 1s decreased from 35 to 15%, 29 to
 366 15%, and 29 to 12%, respectively, and the decreasing trend was
 367 consistent with the findings from C 1s (Figure 1d–i and Table
 368 S2). The peak of Hg at 101.6 eV was assigned to complexes of
 369 $(-\text{COO})_2\text{Hg}$ (Figure S1).^{19,40} These results confirm a similar
 370 Hg adsorption mechanism for activated carbon, biochar_{walnut}
 371 and wildfire ash 1 that involves the formation of complexes
 372 between Hg and oxygen-containing functional groups,
 373 especially the $-\text{COO}$ group.

374 Unlike biochar_{walnut} and wildfire ash 1, Hg adsorption by
 375 activated carbon resulted in a decrease of C content in the C=
 376 C group by 14% (Figure 1d), suggesting that Hg removal by
 377 activated carbon was also attributed to the formation of Hg-
 378 C π bonds.⁴⁰ Previous studies demonstrated that delocalized
 379 lone-pair π electrons were associated with graphite-like
 380 domains of plant-derived biochars.^{41,42} We found that the
 381 quantity of π - π groups in biochar_{walnut} decreased substantially
 382 from 21 to 4.2% (Figure 1e), indicating that π electrons may
 383 be involved in the removal of Hg onto the biochar_{walnut}.
 384 However, electrostatic interactions seem unlikely to be
 385 involved when the dominant Hg species is uncharged
 386 Hg(OH)₂.⁴³ This suggests two possible alternative sorption
 387 mechanisms: (i) π electrons could be involved in the reduction
 388 of Hg(II) to Hg(I) on the C surfaces,^{43,44} and/or (ii) Hg(II)
 389 might complex with C=C and C=O to form Hg- π binding
 390 between Hg and a graphite-like structure (C=C) and C=O
 391 in biochars.¹⁹ Notably, the C content in the C=O group
 392 decreased by 6% in biochar_{walnut} after Hg adsorption (Figure
 393 1e). Like biochar_{walnut}, the peak of π - π bonds for wildfire ash 1
 394 decreased from 8 to 4% after Hg adsorption, suggesting that π
 395 electrons may also be involved in Hg removal by wildfire ash 1.

396 Unlike activated carbon and biochar_{walnut}, the O content in
 397 the C-O/ $-\text{OH}$ group decreased by 35%, and the C=O
 398 group increased by 52% after Hg adsorption by wildfire ash 1
 399 (Figure 1i). These shifts infer that phenolic hydroxyl groups
 400 might participate in the reduction of Hg(II) during Hg
 401 adsorption by wildfire ash 1, consistent with the adsorption
 402 mechanism proposed for bagasse biochar in which the
 403 reduction of Hg(II) by phenol was involved in Hg removal.¹⁹
 404 Thus, considering Hg(OH)₂ as the dominant Hg species in
 405 this work at pH > 7,⁴³ Hg adsorption to the contrasting
 406 sorbent materials is posited as: (i) carboxylic and graphite-like

structures were the predominant binding sites for activated
 carbon; (ii) carboxylic and π electrons were the major binding
 sites for biochar_{walnut}; and (iii) carboxylic and phenolic
 hydroxyl groups were the primary binding sites for wildfire
 ash 1.

Aqueous Sorption of Hg(II). In the absence of added
 Hg(II), there were noticeable changes in DOC concentrations
 in the presence of activated carbon, biochar_{walnut}, biochar_{sawdust},
 wildfire ash 1, and wildfire ash 2 for the different initial DOC
 levels (i.e., low-, mid-, and high-DOC) (Figure 2). Specifically,

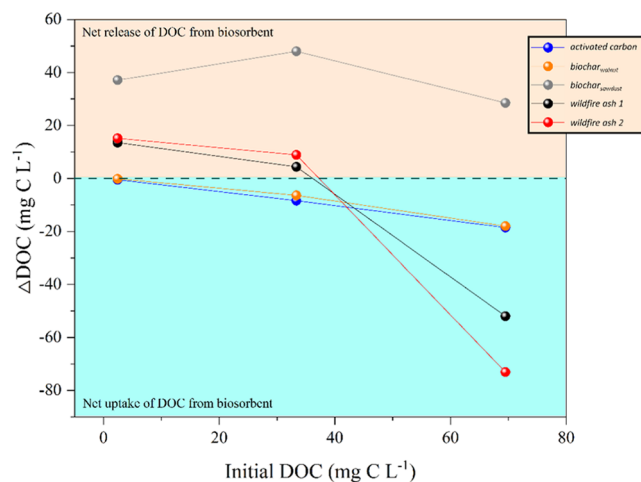


Figure 2. Change of DOC (ΔDOC) per unit mass of carbon in different solid sorbents (i.e., biosorbent stated in the graph) in water of different initial DOC levels (low-DOC: 2.4 mg C L^{-1} ; mid-DOC: 33.4 mg C L^{-1} ; high-DOC: 69.5 mg C L^{-1}) after 48 h.

in low-DOC water, all sorbents, except activated carbon and
 biochar_{walnut} showed a net release of DOC. In mid-DOC
 water, the magnitude of net DOC uptake increased for
 activated carbon and biochar_{walnut} whereas the net DOC
 release was reduced for wildfire ash 1 and wildfire ash 2. In
 high-DOC water, all sorbents, except biochar_{sawdust} showed a
 strong net uptake of DOC from the solution (Figure 2). Only
 activated carbon and biochar_{walnut} consistently retained DOC
 at all of the DOC levels tested. Such DOC-dependent
 properties for DOC release/uptake by the solid-phase sorbents
 are especially important for determining aqueous Hg(II)
 removal as DOM (through thiol groups) forms strong soluble
 Hg complexes in natural waters.

Aqueous Hg(II) adsorption by activated carbon, two
 biochars (biochar_{walnut} and biochar_{sawdust}), four laboratory-
 controlled burn ash (250py, 250ox, 550py, 550ox), and two
 wildfire ash (wildfire ash 1 and wildfire ash 2) samples are
 shown in Figure 3 and Table S3. Notably, both “natural”
 wildfire ash samples exhibited a similar equilibrium adsorption
 capacity (q_e) to activated carbon and biochar_{walnut} in low-DOC
 water (Figure 3 and Table S3). Clearly, DOC had strong
 effects on the q_e of wildfire ash when compared to that of
 activated carbon and biochar_{walnut} (Figure 3 and Table S3).
 Interestingly, both natural wildfire ash samples had significantly
 higher q_{ec} values (expressed as Hg sorbed per unit mass of C)
 ($p < 0.05$) than activated carbon and the two biochars tested
 (Table S3), which may result from Hg(II) being bound by
 sorption or coprecipitation with mineral components, rather
 than exclusively with organic moieties (Table S1),^{46,47} in 445

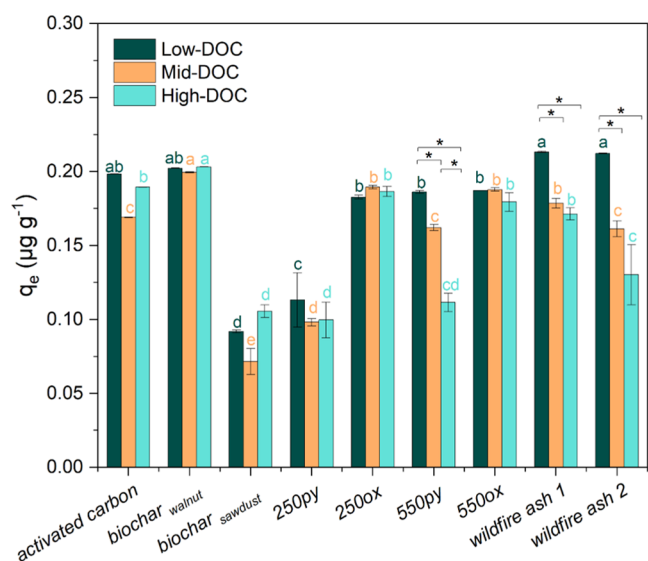


Figure 3. Adsorption capacity of Hg(II) by activated carbon, $\text{biochar}_{\text{walnut}}$, $\text{biochar}_{\text{sawdust}}$, lab-controlled-burn ash (250py, 250ox, 550py, and 550ox), wildfire ash 1, and wildfire ash 2 under different DOC level waters (low-DOC, mid-DOC, and high-DOC) spiked with $1 \mu\text{g L}^{-1}$ of Hg(II). The asterisk above the bars indicates a significant difference of the same adsorbents among different DOC water treatments (one-way ANOVA, * means $p < 0.05$, without * means $p > 0.05$), and the values that are statistically different ($p < 0.05$) among treatments with different solid sorbents under the same DOC level according to one-way ANOVA are indicated by lowercase letters. q_e indicates the equilibrium quantity of adsorbed Hg(II) on per unit mass of sorbent. Error bars represent standard deviation.

addition to potential interactions with the black carbon 446 fraction of the wildfire ash samples.⁹ 447

For the laboratory-controlled burn ash, the material 448 generated under oxidation conditions ($0.18\text{--}0.19 \mu\text{g g}^{-1}$ at 449 250 and 550 °C) had significantly higher q_e values than ash 450 produced under pyrolysis ($0.10\text{--}0.11 \mu\text{g g}^{-1}$ at 250 °C and 451 $0.11\text{--}0.18 \mu\text{g g}^{-1}$ at 550 °C) ($p < 0.05$) (Figure 3 and Table 452 S3). The wildfire ash and laboratory-controlled burn ash 453 displayed quite different q_e values, with wildfire ash 1 and 454 wildfire ash 2 being significantly higher than those of 250py 455 and 550py ash samples ($p < 0.05$) but similar to those of 250ox 456 and 550ox ($p > 0.05$). Consistently, wildfire ash 1, wildfire ash 457 2, and 550py all showed a significant declining trend of q_e 458 values with increasing DOC (Figure 3 and Table S3), 459 indicating a competition between DOM and the solid-phase 460 sorbents for aqueous Hg(II). This corroborates previous 461 observations of a negative relationship between DOM 462 concentration and sorbent removal of Hg(II).^{22,23} 463

To further evaluate the q_e of activated carbon, two biochars, 464 and two wildfire ash samples, sorption isotherms for Hg(II) 465 were determined. The q_e of all sorbents linearly increased with 466 increasing initial Hg(II) concentration (C_0) for all three DOC 467 levels (Figure S3). The Langmuir model well described the 468 sorption isotherms for all sorbents, except for a low r^2 value for 469 $\text{biochar}_{\text{sawdust}}$ in high-DOC water (Table S4). The strong 470 Langmuir model fit suggests that the adsorption process for 471 Hg(II) by these sorbents proceeds as a monolayer adsorption 472 phenomenon.²⁹ Notably, the theoretical adsorption capacity 473 (q_m) for Hg(II) on wildfire ash 1 ($15.5 \mu\text{g g}^{-1}$) and wildfire ash 474 2 ($12.2 \mu\text{g g}^{-1}$) in mid-DOC water was similar to that of 475 activated carbon ($13.9 \mu\text{g g}^{-1}$), but much higher than for both 476

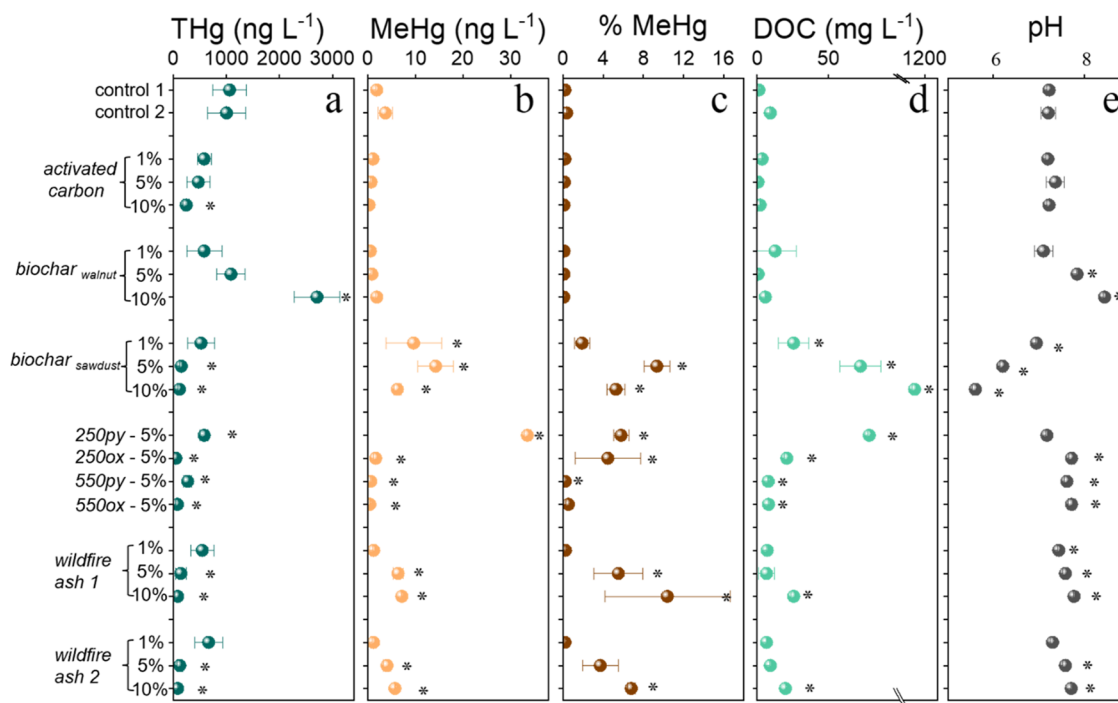


Figure 4. Effects of activated carbon, $\text{biochar}_{\text{walnut}}$, $\text{biochar}_{\text{sawdust}}$, lab-controlled burn ash (250py, 250ox, 550py, and 550ox), wildfire ash 1, and wildfire ash 2 on (a) filtered THg, (b) filtered MeHg, (c) % MeHg, (d) DOC, and (e) pH after 14 days of anoxic sediment incubation. The 1, 5, and 10% contents indicate the amendment level of solid sorbents with sediments. Two independent control samples (control 1 for activated carbon, biochar, and wildfire ash incubations and control 2 for lab-controlled burn ash incubations) were included. Each bars are standard deviation for triplicate samples. Asterisk indicates significantly different values from control based on one-way ANOVA ($p < 0.05$) and Student–Newman–Keuls comparisons.

477 biochar samples ($<5 \mu\text{g g}^{-1}$) (Table S4). These results clearly
478 indicate the strong Hg(II) sorption characteristics by activated
479 carbon and the wildfire ash materials even in the presence of
480 natural DOM.

481 Finally, kinetic experiments demonstrated that 96% of
482 Hg(II) was quickly removed in the first 0.5 h by biochar_{walnut}
483 whereas 94% of Hg(II) was removed by wildfire ash 1 and
484 wildfire ash 2 in the first 4 hours. In contrast, only 91% of
485 Hg(II) was removed by activated carbon after 12 h (Figure
486 S3). In low-DOC water, $>90\%$ of Hg(II) was removed in the
487 first 0.5 h by all materials except for biochar_{sawdust} (Figure
488 S3), but a longer time would be required to remove 90% of Hg(II)
489 in higher DOC waters, revealing that the presence of ambient
490 DOM slows Hg(II) sorption by biosorbents.^{22,23} Meanwhile,
491 when we carried out kinetic studies in high-DOC water, the
492 Hg adsorption rate increased rapidly in the first 1 h for wildfire
493 ash 1 and wildfire ash 2, but then decreased during the
494 following hours before achieving an apparent equilibrium after
495 48 h (Figure S3). We ascribe the rapid initial rate of aqueous
496 sorption during the first hour to the adsorption of labile
497 Hg(II), whereas subsequent release of DOM from the sorbent
498 resulted in competition and a slowing sorption process.
499 Similarly, the net release of DOM from biochar_{sawdust} (Figure
500 2) may be responsible for the lack of Hg(II) reaching
501 equilibrium during the 48 h equilibration period. These
502 findings further demonstrate the importance of DOM as a
503 strong competing ligand for Hg(II) complexation with the
504 binding sites on the solid-phase sorbents.

505 **Effect of Solid Sorbents on Sedimentary Mercury**
506 **Mobilization and Methylation.** Relatively high levels of
507 Hg(II) were mobilized from the Hg-contaminated South River
508 sediments after 14 days of sealed incubation, with an average
509 filtered THg concentration of 1033 ng L^{-1} . The addition of
510 solid-phase sorbents (1, 5, and 10% addition levels) reduced
511 filtered THg concentrations to a range from 52 to 669 ng L^{-1} ,
512 with the exception of the 10% biochar_{walnut} treatment in which
513 filtered THg concentration strikingly increased to 2710 ng L^{-1}
514 (Figure 4 and Table S5). At the 5% addition level, the sorbents
515 displayed the following order in reducing filtered THg during
516 the 2 week anoxic incubation: $250\text{ox} \sim 550\text{ox} > \text{wildfire ash 2}$
517 $\sim \text{wildfire ash 1} \sim \text{biochar}_{\text{sawdust}} > \text{activated carbon} \sim 550\text{py} \sim$
518 $250\text{py} \gg \text{biochar}_{\text{walnut}}$. In general, as the sorbent addition level
519 increased, the filtered THg concentrations decreased for
520 activated carbon (by 45 and 77%; 5 and 10% addition relative
521 to the control, respectively), biochar_{sawdust} (by 37 and 92%),
522 wildfire ash 1 (by 48 and 92%), and wildfire ash 2 (by 50 and
523 88%) (Figure 4 and Table S5). In contrast, increasing the
524 addition level of biochar_{walnut} resulted in even higher filtered
525 THg concentrations (Figure 4) that we attribute, in part, to the
526 increase of pH (from 7.1 to 8.5) with increasing biochar_{walnut}
527 levels as desorption of soil Hg(II) has been shown to increase
528 with increasing pH values from 7 to 9.⁴⁸ In general, both
529 biochar and wildfire ash materials can be alkaline (pH 9–12),
530 with the pH values increasing as the production temperature
531 increases.⁴⁹ We also observed a strong inverse, nonlinear
532 relationship between (filtered) THg and DOC in the
533 treatments with the two wildfire ash samples (Figure S4a),
534 implying potential decoupling of DOM and Hg(II) in the
535 dissolved phase under anoxic conditions.

536 Among laboratory-controlled burn ash samples, the 5%
537 addition level of 250ox and 550ox reduced THg by 95 and
538 92% (compared to control), respectively, which were
539 considerably more effective than the corresponding pyrolysis

540 counterparts of 250py (by 42%) and 550py (by 73%) (Table
541 S5). Notably, a significantly higher aromatic hydrocarbon
542 content was detected in 250ox ($45.0 \pm 3.4\%$), 550ox ($50.8 \pm$
543 3.7%), and 550py ($52.0 \pm 5.1\%$) than that in 250py ($25.9 \pm$
544 3.9%) (data from Chen et al., in review), possibly implying a
545 role for aromatic hydrocarbon compounds in reducing Hg(II)
546 mobilization from the contaminated sediment. These findings
547 corroborated the findings of Ku et al.⁹ in which higher
548 aromatic hydrocarbon content materials tended to limit Hg
549 release to the aqueous phase. Moreover, the ash produced
550 under oxidation conditions (i.e., in the presence of oxygen and
551 a high temperature of 450–1400 °C) was more effective in
552 sequestering sedimentary Hg(II) than ash produced under
553 pyrolysis conditions (i.e., under limited oxygen and a lower
554 temperature from 250 to 450 °C).²⁵

555 In contrast to the high Hg mobilization from sediments, the
556 control treatment resulted in relatively low levels of filtered
557 MeHg (1.8 and 3.7 ng L^{-1}), and the various solid-phase
558 sorbent addition showed variable effectiveness in reducing
559 (filtered) MeHg concentrations (Figure 4 and Table S5). The
560 activated carbon and two of the laboratory-controlled burn ash
561 samples (550py and 550ox) reduced MeHg levels in the
562 incubated samples, whereas the other sorbents produced no
563 effect or even slightly promoted MeHg concentrations in the
564 aqueous phase. The stimulation of MeHg production seems
565 contradictory to the ash-only incubation study by Ku et al.⁹ in
566 which the authors observed little Hg(II) and MeHg in the
567 aqueous phase; we believe that the presence of a contaminated
568 sediment in the current study would provide much more
569 bioavailable Hg(II) and labile organic matter, and these
570 conditions would be more stimulative to Hg(II) methylation
571 than ash-only conditions. The higher aqueous MeHg
572 concentrations may be associated with the higher DOC
573 concentrations in wildfire ash 1 ($r^2 = 0.622$; $p < 0.05$) and
574 wildfire ash 2 ($r^2 = 0.707$; $p < 0.05$) treatments (Figure S4b).
575 Previous studies have demonstrated that DOC can be utilized
576 by microbial Hg methylators as an electron donor to facilitate
577 conversion of Hg(II) to MeHg.^{50,51}

578 Possible reasons for such a low percentage of MeHg yield
579 include the relatively low organic matter content (loss-on-
580 ignition measured at 7%)⁵² of the relatively coarse,
581 contaminated sediments that may limit microbial activity,
582 and also the very high background Hg levels in the sediment
583 that resulted in only a small fractional conversion of THg to
584 MeHg. Another potential reason would be the inhibition of
585 MeHg production due to elevated THg sedimentary levels
586 ($13.4 \mu\text{g g}^{-1}$) as a field study in the historic Hg mining area in
587 Yolo County, California, observed decreasing MeHg with
588 increasing THg in sediments above the THg level of $17 \mu\text{g}$
589 g^{-1} .⁵³

590 Consistent with published data from another sorbent
591 addition study,¹³ bulk sediment THg concentrations were
592 not a good predictor of the effectiveness of sorbents, but
593 sedimentary MeHg concentrations in biochar_{sawdust}, wildfire ash
594 1, wildfire ash 2, and 250py additions were 42, 97, 85, and
595 103% higher than controls (Table S6). Previous studies have
596 demonstrated that the increase in sedimentary MeHg with
597 sorbent addition could have arisen from higher rates of gross
598 MeHg production or reduced MeHg efflux to overlying
599 water.^{13,23} Notably, the partition coefficients of MeHg ($\log K_d$
600 MeHg) in sediments with additions of biochar_{sawdust}, wildfire
601 ash 1, wildfire ash 2, and 250py were not significantly different
602 from the control treatment ($p > 0.05$) (Figure S5). However,

603 with higher log K_d of Hg(II) (Figure S5) and whole microcosm
604 percentage of MeHg (i.e., both water and sediment) (Figure
605 S6) being observed in treatments with biochar_{sawdust} wildfire
606 ash 1, wildfire ash 2, and 250pp, the results may imply that
607 these sorbents may disproportionately increase the availability
608 of Hg(II) for microbial Hg methylators and may result in
609 higher Hg(II) methylation yields under elevated DOC
610 conditions.^{54,55} Direct study of DOM characteristics and
611 microbial Hg(II) methylation⁵⁶ of these incubation samples
612 will be needed to better understand the complex biogeochem-
613 ical processes.

614 It is worth noting that Hg methylation trends in the present
615 study were limited to a relatively short term (2 weeks). Despite
616 the strong sorption toward Hg(II) by wildfire ash, which
617 contributes to the inhibition of MeHg production, on the other
618 hand, the nutrients released by ash⁴ may aid in promoting
619 microbial MeHg production as indicated by the MeHg data,
620 and perhaps MeHg can be degraded in the longer term.⁵⁴
621 Therefore, the ecological risk of wildfire to the downstream
622 water environment in the long term is still entirely unclear and
623 needs further investigation.

624 **Environmental Implications.** This work demonstrates
625 that ash produced by wildfire and prescribed burning has a
626 significant impact on aquatic Hg cycling processes by
627 sequestering aqueous Hg, mediating sedimentary Hg mobi-
628 lization, and altering its conversion to highly toxic MeHg.
629 Wildfire ash materials are readily transported to aquatic
630 systems through runoff/erosion and hydrologic transport
631 following wildfires.²⁴ Per unit mass of bulk or C content, we
632 found that wildfire ash had the highest sorption capabilities for
633 aqueous Hg(II), as compared to activated carbon and selected
634 biochars. The Hg adsorption mechanisms appear to differ
635 among the sorbents evaluated: (i) carboxylic and graphite-like
636 structures were the predominant binding sites for activated
637 carbon; (ii) carboxylic and π electrons were the major binding
638 sites for biochar_{walnut}; and (iii) carboxylic and phenolic
639 hydroxyl groups were the primary binding sites for wildfire
640 ash. DOM leaching from some sorbent materials reduced their
641 net Hg sequestration effectiveness owing to competition for
642 aqueous Hg(II) between the solid-phase sorbents and
643 aqueous-phase DOM.

644 While the effectiveness of activated carbon for inhibiting
645 MeHg production and bioaccumulation in Hg-contaminated
646 aquatic ecosystems has been previously demonstrated,^{13,14} we
647 also confirmed that certain biochars, laboratory-controlled
648 burn ash, and wildfire ash materials altered aqueous Hg(II)
649 levels, bioavailability of Hg(II), and sedimentary Hg
650 methylation. Nevertheless, while wildfire ash can strongly
651 sequester aqueous Hg(II), leaching of its labile organic matter
652 may mobilize sedimentary Hg(II) and/or promote the
653 production of toxic MeHg that can bioaccumulate/biomagnify
654 in downstream aquatic habitats. A similar observation on
655 increased MeHg bioaccumulation was reported in a down-
656 stream lake in Alberta, Canada, after wildfire, partly due to
657 restructuring of food web structure in the lake.⁵⁷ These
658 findings indicate that wildfire ash, especially those generated
659 under low-intensity wildfire (i.e., resulting in black ash), can
660 have appreciable effects on Hg cycling processes in aquatic
661 ecosystems (rivers, wetlands, reservoirs, lakes) and should be
662 considered in post-fire aquatic ecosystem restoration activities
663 and also within the context of the global Hg cycle.⁵⁸ In
664 addition to the increasing adoption of prescribed burning,
665 wildfire impacts on aquatic Hg cycling are expected to greatly

increase as the number, size, and intensity of wildfires rapidly
increase with climate change.

■ ASSOCIATED CONTENT

Supporting Information

The Supporting Information is available free of charge at
<https://pubs.acs.org/doi/10.1021/acs.est.2c01591>.

Tabulated information on the physical and chemical
properties of the solid sorbents, spectroscopic character-
ization of the sorbent surfaces before and after sorption
with aqueous Hg(II), equilibrium quantity of adsorbed
Hg(II) in aqueous sorption tests, isotherm model
parameters for Hg(II), and sealed sediment incubation
data; graphical illustration of XPS spectra, equilibrium
adsorption capacity of Hg(II) at different initial Hg(II)
concentrations, effect of contact time on Hg(II)
adsorption, and relationships between DOC and Hg(II)
or MeHg after 2 weeks of sediment incubation (PDF)

■ AUTHOR INFORMATION

Corresponding Authors

Martin Tsz-Ki Tsui – Department of Biology, University of
North Carolina at Greensboro, Greensboro, North Carolina
27402, United States; School of Life Sciences, State Key
Laboratory of Agrobiotechnology, The Chinese University of
Hong Kong, Shatin, NT 999077 Hong Kong SAR, China;
orcid.org/0000-0003-2002-1530; Phone: +852-
39436123; Email: mtktsui@cuhk.edu.hk; Fax: +852-
26037246

Zhang Cheng – College of Environmental Science, Sichuan
Agricultural University, Chengdu 611130, China;
orcid.org/0000-0001-6211-3017; Email: cz@sicau.edu.cn

Xue-Mei Zhu – College of Environmental Science, Sichuan
Agricultural University, Chengdu 611130, China;
Email: zhuxuemei@sicau.edu.cn

Authors

Han-Han Li – College of Environmental Science, Sichuan
Agricultural University, Chengdu 611130, China;
Department of Biology, University of North Carolina at
Greensboro, Greensboro, North Carolina 27402, United
States

Peijia Ku – Department of Biology, University of North
Carolina at Greensboro, Greensboro, North Carolina 27402,
United States; Environmental Sciences Division, Oak Ridge
National Laboratory, Oak Ridge, Tennessee 37830, United
States; orcid.org/0000-0003-2813-9269

Huan Chen – Biogeochemistry & Environmental Quality
Research Group, Clemson University, Georgetown, South
Carolina 29442, United States; orcid.org/0000-0001-9998-1205

Ziyu Yin – Department of Nanoscience, Joint School of
Nanoscience and Nanoengineering, University of North
Carolina at Greensboro, Greensboro, North Carolina 27401,
United States

Randy A. Dahlgren – Department of Land, Air and Water
Resources, University of California, Davis, California 95616,
United States

Sanjai J. Parikh – Department of Land, Air and Water
Resources, University of California, Davis, California 95616,
United States

725 **Jianjun Wei** – Department of Nanoscience, Joint School of
726 Nanoscience and Nanoengineering, University of North
727 Carolina at Greensboro, Greensboro, North Carolina 27401,
728 United States; orcid.org/0000-0002-2658-0248
729 **Tham C. Hoang** – School of Fisheries, Aquaculture and
730 Aquatic Sciences, Auburn University, Auburn, Alabama
731 36849, United States
732 **Alex T. Chow** – Biogeochemistry & Environmental Quality
733 Research Group, Clemson University, Georgetown, South
734 Carolina 29442, United States; orcid.org/0000-0001-7441-8934
735

736 Complete contact information is available at:
737 <https://pubs.acs.org/10.1021/acs.est.2c01591>

738 Notes

739 The authors declare no competing financial interest.

740 ■ ACKNOWLEDGMENTS

741 The authors acknowledge the funding support by the China
742 Scholarship Council to H.L. for undertaking this overseas
743 exchange program. This study was financially supported by the
744 National Science Foundation awards (EAR-1711642 and
745 CBET-1917156) and the National Institute of Food and
746 Agriculture award (2018-67019-27795) both to M.T.-K.T. and
747 A.T.C.

748 ■ REFERENCES

749 (1) Scharenbroch, B. C.; Nix, B.; Jacobs, K. A.; Bowles, M. L. Two
750 decades of low-severity prescribed fire increases soil nutrient
751 availability in a Midwestern, USA oak (*Quercus*) forest. *Geoderma*
752 **2012**, *183*, 183–184, 80–91.
753 (2) Westerling, A. L.; Hidalgo, H. G.; Cayan, D. R.; Swetnam, T. W.
754 Warming and earlier spring increase western US forest wildfire
755 activity. *Science* **2006**, *313*, 940–943.
756 (3) Francos, M.; Úbeda, X. Prescribed fire management. *Curr. Opin.*
757 *Environ. Sci. Health* **2021**, *21*, No. 100250.
758 (4) Rhoades, C. C.; Chow, A. T.; Covino, T. P.; Feghel, T. S.;
759 Pierson, D. N.; Rhea, A. E. The legacy of a severe wildfire on stream
760 nitrogen and carbon in headwater catchments. *Ecosystems* **2019**, *22*,
761 643–657.
762 (5) Fitzgerald, W. F.; Engstrom, D. R.; Mason, R. P.; Nater, E. A.
763 The case for atmospheric mercury contamination in remote areas.
764 *Environ. Sci. Technol.* **1998**, *32*, 1–7.
765 (6) St Louis, V. L.; Rudd, J. W. M.; Kelly, C. A.; Hall, B. D.; Rolffhus,
766 K. R.; Scott, K. J.; Lindberg, S. E.; Dong, W. Importance of the forest
767 canopy to fluxes of methyl mercury and total mercury to boreal
768 ecosystems. *Environ. Sci. Technol.* **2001**, *35*, 3089–3098.
769 (7) Webster, J. P.; Kane, T. J.; Obrist, D.; Ryan, J. N.; Aiken, G. R.
770 Estimating mercury emissions resulting from wildfire in forests of the
771 Western United States. *Sci. Total Environ.* **2016**, *568*, 578–586.
772 (8) Tuhý, M.; Rohovec, J.; Matoušková, S.; Mihaljevič, M.; Kříbek,
773 B.; Vaněk, A.; Mapani, B.; Göttlicher, J.; Steininger, R.; Majzlan, J.;
774 Ettler, V. The potential wildfire effects on mercury remobilization
775 from topsoils and biomass in a smelter-polluted semi-arid area.
776 *Chemosphere* **2020**, *247*, No. 125972.
777 (9) Ku, P.; Tsui, M. T. K.; Nie, X.; Chen, H.; Hoang, T. C.; Blum, J.
778 D.; Dahlgren, R. A.; Chow, A. T. Origin, reactivity, and bioavailability
779 of mercury in wildfire ash. *Environ. Sci. Technol.* **2018**, *52*, 14149–
780 14157.
781 (10) Regnell, O.; Watras, C. J. Microbial mercury methylation in
782 aquatic environments: A critical review of published field and
783 laboratory studies. *Environ. Sci. Technol.* **2019**, *53*, 4–19.
784 (11) Lavoie, R. A.; Jardine, T. D.; Chumchal, M. M.; Kidd, K. A.;
785 Campbell, L. M. Biomagnification of mercury in aquatic food webs: A
786 worldwide meta-analysis. *Environ. Sci. Technol.* **2013**, *47*, 13385–
787 13394.

(12) Huang, C. P.; Blankenship, D. W. The removal of mercury(II) 788
from dilute aqueous solution by activated carbon. *Water Res.* **1984**, 789
18, 37–46. 790
(13) Gilmour, C. C.; Riedel, G. S.; Riedel, G.; Kwon, S.; Landis, R.; 791
Brown, S. S.; Menzie, C. A.; Ghosh, U. Activated carbon mitigates 792
mercury and methylmercury bioavailability in contaminated sedi- 793
ments. *Environ. Sci. Technol.* **2013**, *47*, 13001–13010. 794
(14) Gilmour, C.; Bell, T.; Soren, A.; Riedel, G.; Riedel, G.; Kopec, 795
D.; Bodaly, D.; Ghosh, U. Activated carbon thin-layer placement as an 796
in situ mercury remediation tool in a Penobscot River salt marsh. *Sci.* 797
Total Environ. **2018**, *621*, 839–848. 798
(15) Ranganathan, K. Adsorption of Hg(II) ions from aqueous 799
chloride solutions using powdered activated carbons. *Carbon* **2003**, 800
41, 1087–1092. 801
(16) Zabihi, M.; Ahmadpour, A.; Asl, A. H. Removal of mercury 802
from water by carbonaceous sorbents derived from walnut shell. *J.* 803
Hazard. Mater. **2009**, *167*, 230–236. 804
(17) Gomez-Eyles, J. L.; Yupanqui, C.; Beckingham, B.; Riedel, G.; 805
Gilmour, C.; Ghosh, U. Evaluation of biochars and activated carbons 806
for *in situ* remediation of sediments impacted with organics, mercury, 807
and methylmercury. *Environ. Sci. Technol.* **2013**, *47*, 13721–13729. 808
(18) Boutsika, L. G.; Karapanagioti, H. K.; Manariotis, I. D. Aqueous 809
mercury sorption by biochar from malt spent rootlets. *Water Air Soil* 810
Pollut. **2014**, *225*, 1–10. 811
(19) Xu, X.; Schierz, A.; Xu, N.; Cao, X. Comparison of the 812
characteristics and mechanisms of Hg(II) sorption by biochars and 813
activated carbon. *J. Colloid Interface Sci.* **2016**, *463*, 55–60. 814
(20) Wang, A. O.; Ptacek, C. J.; Blowes, D. W.; Gibson, B. D.; 815
Landis, R. C.; Dyer, J. A.; Ma, J. Application of hardwood biochar as a 816
reactive capping mat to stabilize mercury derived from contaminated 817
floodplain soil and riverbank sediments. *Sci. Total Environ.* **2019**, 818
652, 549–561. 819
(21) Wang, Y.; Sun, Y.; He, T.; Deng, H.; Wang, Z.; Wang, J.; 820
Zheng, X.; Zhou, L.; Zhong, H. Biochar amendment mitigates the 821
health risks of dietary methylmercury exposure from rice consumption 822
in mercury-contaminated areas. *Environ. Pollut.* **2020**, *267*, 823
No. 115547. 824
(22) Johs, A.; Eller, V. A.; Mehlhorn, T. L.; Brooks, S. C.; Harper, D. 825
P.; Mayes, M. A.; Pierce, E. M.; Peterson, M. J. Dissolved organic 826
matter reduces the effectiveness of sorbents for mercury removal. *Sci.* 827
Total Environ. **2019**, *690*, 410–416. 828
(23) Schwartz, G. E.; Sanders, J. P.; McBurney, A. M.; Brown, S. S.; 829
Ghosh, U.; Gilmour, C. C. Impact of dissolved organic matter on 830
mercury and methylmercury sorption to activated carbon in soils: 831
Implications for remediation. *Environ. Sci.: Processes Impacts* **2019**, *21*, 832
485–496. 833
(24) Uzun, H.; Dahlgren, R. A.; Olivares, C.; Erdem, C. U.; Karanfil, 834
T.; Chow, A. T. Two years of post-wildfire impacts on dissolved 835
organic matter, nitrogen, and precursors of disinfection by-products in 836
California stream waters. *Water Res.* **2020**, *181*, No. 115891. 837
(25) Bodí, M. B.; Martín, D. A.; Balfour, V. N.; Santín, C.; Doerr, S. 838
H.; Pereira, P.; Cerdà, A.; Mataix-Solera, J. Wildland fire ash: 839
Production, composition and eco-hydro-geomorphic effects. *Earth-Sci.* 840
Rev. **2014**, *130*, 103–127. 841
(26) Wang, J. J.; Dahlgren, R. A.; Chow, A. T. Controlled burning of 842
forest detritus altering spectroscopic characteristics and chlorine 843
reactivity of dissolved organic matter: Effects of temperature and 844
oxygen availability. *Environ. Sci. Technol.* **2015**, *49*, 14019–14027. 845
(27) Mukome, F. N. D.; Zhang, X.; Silva, L. C.; Six, J.; Parikh, S. J. 846
Use of chemical and physical characteristics to investigate trends in 847
biochar feedstocks. *J. Agric. Food Chem.* **2013**, *61*, 2196–2204. 848
(28) USEPA. *Methods for Measuring the Acute Toxicity of Effluents* 849
and Receiving Waters to Freshwater and Marine Organisms; US 850
Environmental Protection Agency: Washington, DC, USA, 2002. 851
(29) Fang, R.; Lu, C.; Zhong, Y.; Xiao, Z.; Liang, C.; Huang, H.; 852
Gan, Y.; Zhang, J.; Pan, G.; Xia, X.; Xia, Y.; Zhang, W. Puffed rice 853
carbon with coupled sulfur and metal iron for high-efficiency mercury 854
removal in aqueous solution. *Environ. Sci. Technol.* **2020**, *54*, 2539– 855
2547. 856

- 857 (30) Tsui, M. T. K.; Finlay, J. C.; Nater, E. A. Effects of stream water
858 chemistry and tree species on release and methylation of mercury
859 during litter decomposition. *Environ. Sci. Technol.* **2008**, *42*, 8692–
860 8697.
- 861 (31) Chow, E.; Tsui, M. T. K. Elucidating microbial pathways of
862 mercury methylation during litter decomposition. *Bull. Environ.*
863 *Contam. Toxicol.* **2019**, *103*, 617–622.
- 864 (32) Washburn, S. J.; Blum, J. D.; Demers, J. D.; Kurz, A. Y.; Landis,
865 R. C. Isotopic characterization of mercury downstream of historic
866 industrial contamination in the South River, Virginia. *Environ. Sci.*
867 *Technol.* **2017**, *51*, 10965–10973.
- 868 (33) Woerndle, G. E.; Tsui, M. T. K.; Sebestyen, S. D.; Blum, J. D.;
869 Nie, X.; Kolka, R. K. New insights on ecosystem mercury cycling
870 revealed by stable isotopes of mercury in water flowing from a
871 headwater peatland catchment. *Environ. Sci. Technol.* **2018**, *52*, 1854–
872 1861.
- 873 (34) Parker, J. L.; Bloom, N. S. Preservation and storage techniques
874 for low-level aqueous mercury speciation. *Sci. Total Environ.* **2005**,
875 *337*, 253–263.
- 876 (35) Mitchell, C. P. J.; Branfireun, B. A.; Kolka, R. K. Spatial
877 characteristics of net methylmercury production hot spots in
878 peatlands. *Environ. Sci. Technol.* **2008**, *42*, 1010–1016.
- 879 (36) Khan, T. A.; Khan, E. A.; Shahjahan. Removal of basic dyes
880 from aqueous solution by adsorption onto binary iron-manganese
881 oxide coated kaolinite: Non-linear isotherm and kinetics modeling.
882 *Appl. Clay Sci.* **2015**, *107*, 70–77.
- 883 (37) Cerrato, J. M.; Blake, J. M.; Hirani, C.; Clark, A. L.; Ali, A. M.;
884 Artyushkova, K.; Peterson, E.; Bixby, R. J. Wildfires and water
885 chemistry: Effect of metals associated with wood ash. *Environ. Sci.*
886 *Processes Impacts* **2016**, *18*, 1078–1089.
- 887 (38) Wang, J.; Deng, B.; Chen, H.; Wang, X.; Zheng, J. Removal of
888 aqueous Hg(II) by polyaniline: Sorption characteristics and
889 mechanisms. *Environ. Sci. Technol.* **2009**, *43*, 5223–5228.
- 890 (39) Guo, X.; Li, M.; Liu, A.; Jiang, M.; Niu, X.; Liu, X. Adsorption
891 mechanisms and characteristics of Hg²⁺ removal by different fractions
892 of biochar. *Water* **2020**, *12*, No. 2105.
- 893 (40) Dong, X.; Ma, L. Q.; Zhu, Y.; Li, Y.; Gu, B. Mechanistic
894 investigation of mercury sorption by Brazilian pepper biochars of
895 different pyrolytic temperatures based on X-ray photoelectron
896 spectroscopy and flow calorimetry. *Environ. Sci. Technol.* **2013**, *47*,
897 12156–12164.
- 898 (41) Bourke, J.; Manley-Harris, M.; Fushimi, C.; Dowaki, K.;
899 Nunoura, T.; Antal, M. J. Do all carbonized charcoals have the same
900 chemical structure? 2. A model of the chemical structure of
901 carbonized charcoal. *Ind. Eng. Chem. Res.* **2007**, *46*, 5954–5967.
- 902 (42) Harvey, O. R.; Herbert, B. E.; Rhue, R. D.; Kuo, L. J. Metal
903 interactions at the biochar-water interface: Energetics and structure-
904 sorption relationships elucidated by flow adsorption microcalorimetry.
905 *Environ. Sci. Technol.* **2011**, *45*, 5550–5556.
- 906 (43) Sánchez-Polo, M.; Rivera-Utrilla, J. Adsorbent-adsorWate
907 interactions in the adsorption of Cd(II) and Hg(II) on ozonized
908 activated carbons. *Environ. Sci. Technol.* **2002**, *36*, 3850–3854.
- 909 (44) Zhu, J.; Deng, B.; Yang, J.; Gang, D. Modifying activated
910 carbon with hybrid ligands for enhancing aqueous mercury removal.
911 *Carbon* **2009**, *47*, 2014–2025.
- 912 (45) Ravichandran, M. Interactions between mercury and dissolved
913 organic matter—A review. *Chemosphere* **2004**, *55*, 319–331.
- 914 (46) El-Shafey, E. I. Removal of Zn(II) and Hg(II) from aqueous
915 solution on a carbonaceous sorbent chemically prepared from rice
916 husk. *J. Hazard. Mater.* **2010**, *175*, 319–327.
- 917 (47) Kong, H.; He, J.; Gao, Y.; Wu, H.; Zhu, X. Cosorption of
918 phenanthrene and mercury(II) from aqueous solution by soybean
919 stalk-based biochar. *J. Agric. Food Chem.* **2011**, *59*, 12116–12123.
- 920 (48) Jing, Y. D.; He, Z. L.; Yang, X. E. Effects of pH, organic acids,
921 and competitive cations on mercury desorption in soils. *Chemosphere*
922 **2007**, *69*, 1662–1669.
- 923 (49) Certini, G. Effects of fire on properties of forest soils: A review.
924 *Oecologia* **2005**, *143*, 1–10.
- (50) Chiasson-Gould, S. A.; Blais, J. M.; Poulain, A. J. Dissolved
925 organic matter kinetically controls mercury bioavailability to bacteria.
926 *Environ. Sci. Technol.* **2014**, *48*, 3153–3161.
- (51) Liu, P.; Ptacek, C. J.; Blowes, D. W. Mercury complexation with
928 dissolved organic matter released from thirty-six types of biochar. *Bull.*
929 *Environ. Contam. Toxicol.* **2019**, *103*, 175–180.
- (52) Ku, P.; Tsui, M. T. K.; Liu, S.; Corson, K. B.; Williams, A. S.;
931 Monteverde, M. R.; Woerndle, G. E.; Hershey, A. E.; Rublee, P. A.
932 Examination of mercury contamination from a recent coal ash spill
933 into the Dan River, North Carolina, United States. *Ecotoxicol. Environ.*
934 *Saf.* **2021**, *208*, No. 111469.
- (53) Holloway, J. M.; Goldhaber, M. B.; Scow, K. M.; Drenovsky, R.
936 E. Spatial and seasonal variations in mercury methylation and
937 microbial community structure in a historic mercury mining area,
938 Yolo County, California. *Chem. Geol.* **2009**, *267*, 85–95.
- (54) Marvin-DiPasquale, M. C.; Oremland, R. S. Bacterial
940 methylmercury degradation in Florida Everglades peat sediment.
941 *Environ. Sci. Technol.* **1998**, *32*, 2556–2563.
- (55) Ullrich, S. M.; Tanton, T. W.; Abdrashitov, S. A. Mercury in the
943 aquatic environment: A review of factors affecting methylation. *Crit.*
944 *Rev. Environ. Sci. Technol.* **2001**, *31*, 241–293.
- (56) Mangal, V.; Stenzler, B. R.; Poulain, A. J.; Guéguen, C. Aerobic
946 and anaerobic bacterial mercury uptake is driven by algal organic
947 matter composition and molecular weight. *Environ. Sci. Technol.* **2019**,
948 *53*, 157–165.
- (57) Kelly, E. N.; Schindler, D. W.; St Louis, V. L.; Donald, D. B.;
950 Vladicka, K. E. Forest fire increases mercury accumulation by fishes
951 via food web restructuring and increased mercury inputs. *Proc. Natl.*
952 *Acad. Sci. U.S.A.* **2006**, *103*, 19380–19385.
- (58) Selin, N. E. Global change and mercury cycling: challenges for
954 implementing a global mercury treaty. *Environ. Toxicol. Chem.* **2014**,
955 *33*, 1202–1210.